AIAA JOURNAL
Vol. 32, No. 1, January 1994

Supersonic Base Flow Experiments in the Near Wake of a Cylindrical Afterbody

J. L. Herrin* and J. C. Dutton†
University of Illinois at Urbana-Champaign, Urbana, Illinois 61801

The near wake of a circular cylinder aligned with a uniform Mach 2.5 flow has been experimentally investigated in a wind tunnel designed solely for this purpose. Mean static pressure measurements were used to assess the radial dependence of the base pressure and the mean pressure field approaching separation. In addition, two-component laser Doppler velocimeter (LDV) measurements were obtained throughout the near wake including the large separated region downstream of the base. The primary objective of the research was to gain a better understanding of the complex fluid dynamic processes found in supersonic base flowfields including separation, shear layer development, reattachment along the axis of symmetry, and subsequent development of the wake. Results indicate relatively large reverse velocities and uniform turbulence intensity levels in the separated region. The separated shear layer is characterized by high turbulence levels with a strong peak in the inner, subsonic region which eventually decays through reattachment as the wake develops. A global maximum in turbulent kinetic energy and Reynolds shear stress is found upstream of the reattachment point, which is in contrast to data from the reattachment of a supersonic shear layer onto a solid wall.

Nomenclature

C_f = skin friction coefficient
C_p = dimensionless pressure coefficient
H = compressible shape factor, δ^*/θ
M = Mach number
k = turbulent kinetic energy
P = pressure
P_k = production of k
R = base radius
r = radial coordinate
S = location of reattachment point
t = tangential coordinate
U = mean axial velocity
u_τ = friction velocity
V_r = mean radial velocity
V_t = mean tangential velocity
x = axial coordinate
y = vertical distance, r-R
γ = ratio of specific heats
δ = boundary-layer thickness
δ^* = displacement thickness
θ = momentum thickness
ν_w = kinematic viscosity at wall
Π = wake strength parameter
σ = root-mean-square value
$< >$ = ensemble-averaged value

Subscripts

base = condition at base
u = axial component
v_r = radial component
v_t = tangential component
1 = condition at nozzle exit

Superscript

$( )'$ = fluctuating value

Introduction

THE low pressures that act in the base region of bodies of revolution in supersonic flight can cause significant amounts of drag.[1] For this reason, practical methods such as boattailing, base bleed, and base burning have been developed to increase the base pressure on aerodynamic vehicles such as missiles, rockets, and projectiles. To further enhance vehicle performance, however, a more complete understanding of the complex fluid dynamic processes that occur in base flowfields is necessary. Past experimental efforts have provided an adequate description of the overall flowfield structure and some parametric trends, but very little detailed quantitative data exists, especially for supersonic flows. In fact, a comprehensive survey of the available experimental data on axisymmetric base flows was recently undertaken by GARTEUR Action Group AG09.[2] After an exhaustive search, the group concluded that no accurate, well-documented experimental data existed for the near-wake flowfield in supersonic, axisymmetric flow. Reliable turbulence information in the base region is especially scarce which presents a problem in validating numerical predictions of these flowfields (see Refs. 3–5). Clearly, the practical importance of increasing the understanding of axisymmetric base flowfields lies in the ability to someday control the near-wake flow interactions such that base drag can be reduced and vehicle stability and control can be enhanced.

A schematic diagram of the mean flowfield structure in the near wake of a cylindrical afterbody aligned with a supersonic flow is shown in Fig. 1. The supersonic afterbody freestream flow undergoes a strong expansion centered at the base corner as the turbulent boundary layer separates geometrically from the body. A free shear layer is formed which separates the outer inviscid flow from a relatively large recirculation region immediately downstream of the base. The intense turbulent mixing and energy exchange that characterize the free shear layer are important in determining the flowfield properties throughout the near wake including the recirculation region. As the free shear layer approaches the axis of symmetry, a recompression process occurs which eventually realigns the flowfield with the axis. A rear stagnation point, where the mean velocity vanishes, is located on the centerline and separates the recirculation region from the wake which develops downstream.

The early theoretical model for turbulent base flows developed by Korst[6] prompted several experimental investigations which at-

Received Nov. 20, 1992; revision received June 6, 1993; accepted for publication July 3, 1993; presented as Paper 93-2924 at the AIAA 24th Fluid Dynamics, Plasma Dynamics, and Lasers Conference, Orlando, FL, July 6–9, 1993.

*Graduate Research Assistant; currently National Research Council Associate, NASA Langley Research Center, M/S 163, Hampton, VA 23681. Member AIAA.

†Professor, Department of Mechanical and Industrial Engineering, 140 Mechanical Engineering Building, 1206 W. Green St. Associate Fellow AIAA.

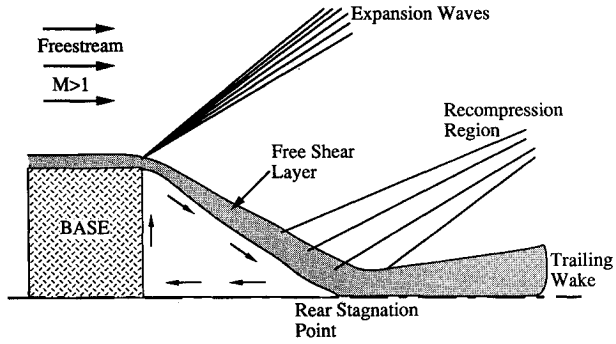

Fig. 1 Supersonic, axisymmetric base flow schematic.

tempted to gather the empirical information necessary to complete the theory.[7–10] However, many experimental problems, including improper model mounting, probe interference effects, and lack of flowfield symmetry, hampered these efforts which resulted in data of questionable accuracy. These experimental difficulties stem primarily from the axisymmetric geometry of the body as well as the sensitivity of the separated region downstream of the base to wind-tunnel interference effects.[11] Perhaps the most comprehensive previous study of supersonic power-off base flows was undertaken by Gaviglio et al.[12] using a hot-wire anemometer. The overall inviscid flow structure and downstream wake properties were determined; however, the recirculation region directly behind the base was not investigated due to possible probe interference effects which limits the utility of the data. Neale et al.[13] investigated the mean velocity field behind a circular cylinder with a pitot-static probe but, again, bypassed the separated region. Clearly, accurate experimental measurements in the recirculation region downstream of the base require nonintrusive diagnostic techniques. Laser Doppler velocimetry (LDV) is a nonintrusive velocity measurement tool well-suited for such flows. Delery[14] used LDV to successfully document the near wake of a subsonic, axisymmetric base flowfield. Detailed mean velocity and turbulence data were gathered throughout the near wake and provide a good data base for the subsonic case. Amatucci et al.[15] made similar LDV measurements in a supersonic, two-stream flowfield with a two-dimensional base that modeled the power-on case; however, the effects of the more practical axisymmetric configuration were not investigated. Heltsley et al.[16] used LDV to investigate the flowfield downstream of a transonic, axisymmetric, power-on base flow but encountered experimental problems throughout the measurements.

In the current study, experiments were conducted to document the entire near-wake flowfield structure behind a cylindrical afterbody immersed in a supersonic flow. Detailed LDV measurements were made to obtain a better understanding of the fluid dynamic processes throughout the near wake including separation, shear layer growth and development, reattachment, and wake redevelopment. To the authors' knowledge, these data also provide the first detailed investigation of the mean and turbulent velocity fields inside the recirculation region in a supersonic base flow. In addition, the data provided herein will aid both analytical and numerical modelers of supersonic, axisymmetric base flows.

Experimental Facility and Instrumentation

Wind Tunnel Facility

The experiments were conducted in a supersonic, blowdown-type wind tunnel designed solely for the study of axisymmetric base flows. Figure 2 is a schematic diagram of the axisymmetric wind-tunnel facility which is located in the University of Illinois Gas Dynamics Laboratory. Dry, compressed air passes from the stagnation chamber through a flow conditioning module consisting of screens and honeycomb (used to dampen any large-scale disturbances generated in the air supply process and to minimize freestream turbulence levels) and finally to the converging-diverging supply nozzle. The pressure and temperature in the stagnation chamber were consistently maintained at 515 ± 2.8 kPa and 294 ± 3 K, respectively. The nozzle takes an annular shape due to the central sting which supports the base model from upstream to prevent any interference with the near-wake flowfield. The cylindrical afterbody used in the present experiments is 63.5 mm in diameter and is attached by internal threads to the sting. Physical supports for the sting are located outside the rear of the stagnation chamber and inside the wind tunnel at the flow conditioning module. The sting supports are of sufficient rigidity such that sting vibration due to flowfield fluctuations was negligible. The nominal design Mach number and unit Reynolds number at the nozzle exit are 2.5 and 52 (10^6) per meter, respectively.

Proper centering of the afterbody/base within the nozzle is critical in obtaining axisymmetric flow in the near wake. In these experiments, custom-designed wind-tunnel adjusting blocks were used to adjust the relative position between the sting and nozzle until an axisymmetric flow was obtained. Oil-streak visualization performed on the base was used effectively to examine the sting/nozzle alignment and was found to be a very sensitive indicator of the symmetry of the near-wake flowfield. Micrometer measurements at the nozzle exit indicated a maximum afterbody misalignment of 0.13 mm from the physical nozzle centerline.

Experimental Methods

Conventional schlieren and shadowgraph photography were used to investigate the qualitative structure of the near-wake flowfield. The photographs were of only moderate quality due to the axisymmetric nature of the flow, but they were used successfully to confirm the flowfield structure shown in Fig. 1 and to determine a proper operating condition that eliminated any wind-tunnel interference effects.

Mean static pressure measurements were made at several locations on the base and afterbody surfaces using a Pressure Systems Inc. digital pressure transmitter (DPT 6400-T). There were 19 pressure taps (0.64 mm in diameter) located symmetrically across the base at radial intervals of 3.18 mm. Along the afterbody, two sets of diametrically opposed pressure taps (0.64 mm in diameter) were located starting 2.38 mm upstream of the base corner with each tap separated axially by 3.18 mm and a total of five taps in each set. In addition to the afterbody pressure taps, total pressure and temperature probes were mounted in the stagnation chamber.

The focus of this investigation involved the implementation of a two-component LDV system for measuring the near-wake velocity field. Artificial seed particles were generated by a TSI Inc. six-jet atomizer filled with 50 cp silicone oil. The droplets were injected into the flow upstream of the facility nozzle to avoid disturbing the flowfield with the injection process. In previous experiments with the same seeding apparatus, Bloomberg[17] deduced a mean droplet diameter of 0.8 μm and showed mean particle relaxation distances

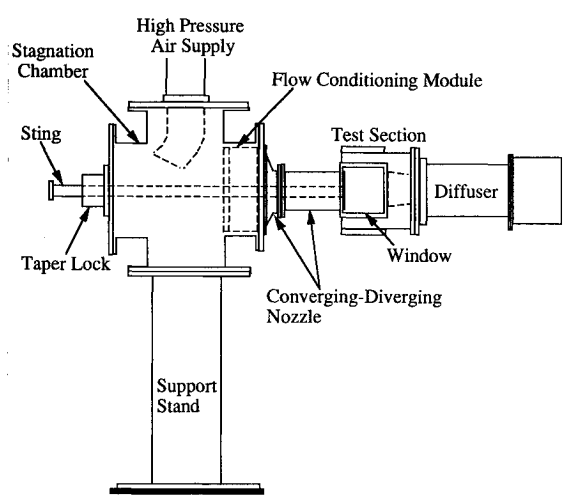

Fig. 2 Schematic diagram of axisymmetric wind tunnel.

of approximately 2 mm downstream of an oblique shock wave generated by a 15-deg compression corner in a Mach 2.6 flow. The maximum velocity gradients in the present experiments (near boundary-layer separation) are significantly weaker than for the oblique shock in Bloomberg's work; however, to ensure negligible particle lag in the current experiments, no data are presented within the first 5 mm downstream of the base corner separation point. In the separated shear layer, the Stokes number for this seeding configuration is estimated to be 0.15 which Samimy and Lele[18] have shown yields root-mean-square slip velocities (difference in velocity between the particle and the local fluid element) of approximately 1.5%.

The LDV measurement volume used in these experiments was 120 μm in diameter and had a fringe spacing of approximately 10.3 μm. A 20-deg off-axis, forward-scatter receiving optics configuration was used to reduce the effective measurement volume length to 0.70 mm. Bragg cells were used in each component to frequency shift one of the beams 40 MHz against the mean flow direction to discriminate reverse velocities. In addition, the two orthogonal fringe patterns were rotated to ±45 deg relative to the wind-tunnel axis to reduce fringe blindness. To measure accurately the Doppler frequencies in this demanding flow, a TSI Inc. IFA-750 autocorrelation processor was used. Data were gathered from the processor by a Gateway 2000 486-33 personal computer where further processing and analysis were performed. Positioning of the LDV measurement volume throughout the near-wake flowfield was accomplished using a three-axis, computer-controlled traversing table with a positioning resolution of 0.75 μm.

The LDV measurement locations were concentrated in the regions of high velocity gradients including the approach boundary layer, separated shear layer, developing wake, and also near the reattachment point. Radial traverses were completed at 21 axial stations throughout the near wake with approximately 30 spatial locations per traverse. In addition, an axial traverse along the model centerline was performed to show the development of the centerline mean velocity and turbulence intensities. During each radial traverse, three or four locations below the axis of symmetry were measured to check the symmetry of the flow. In all cases, the measured wake centerline (defined as the location where $\langle u'v_r' \rangle = 0$) was within 2 mm of the geometric model centerline. Approximately 4000 instantaneous velocity realizations were gathered at each spatial location and probability density functions (pdfs) of each velocity component were calculated. The pdfs generally resembled a Gaussian profile except near the inner edge of the shear layer (near $U = 0$) where bimodal peaks in each pdf consistently occurred. The bimodal pdfs most likely indicate the presence of large-scale structures on the inner edge of the shear layer which play an important role in the entrainment of fluid from the recirculation region. The effects of velocity bias on the LDV data were accounted for by weighting each velocity realization with the interarrival time between realizations.[19]

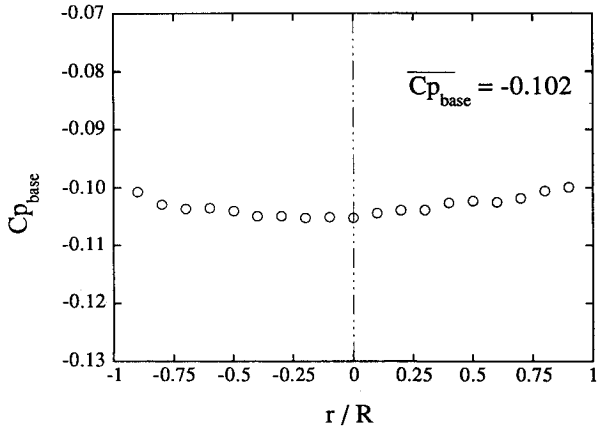

Fig. 3 Base pressure profile.

With the current two-component LDV arrangement, both the horizontal and vertical components of velocity were measured. In two-dimensional flows, this generally allows direct measurement of the streamwise and transverse velocities, but no measurement of the spanwise component. In the current axisymmetric flow, by using the same LDV configuration and making measurements independently in both the horizontal and vertical planes which pass through the axis of symmetry, all three mean and rms velocities have been measured. In addition, the axial-radial ($u'v_r'$) and axial-tangential ($u'v_t'$) Reynolds shear stresses have been directly measured. An error analysis including the uncertainties associated with velocity biasing, fringe biasing, velocity gradient biasing, finite ensemble size, processor resolution, optical misalignment, and fringe spacing determination has been completed. The estimated *worst-case* uncertainty in the mean velocity measurements is 1.2% of U_1 and, in the rms velocity fluctuations, 2.3% of U_1, where U_1 is the freestream velocity just prior to separation.

Results

Pressure Measurements

Static pressure measurements along the afterbody were used to assess the uniformity of the nozzle exit flow as well as any upstream influence of the separation process. As expected, the pressure field approaching the base corner was relatively uniform and takes a value consistent with an isentropically expanded Mach 2.44 flow. No upstream influence from the base corner separation was evident in the data.

Pressure measurements have also been made at 19 locations on the base to assess the radial distribution of the mean static pressure. Figure 3 shows the dimensionless base pressure coefficient at each location, defined as

$$C_{p_{\text{base}}} = \frac{2\left[\left(P_{\text{base}}/P_1\right) - 1\right]}{\gamma M_1^2} \tag{1}$$

where P is the static pressure. The pressure is shown to be relatively constant across the base (note the expanded vertical scale) with a slight increase toward larger radii where the maximum pressure measured was 3.9% higher than the pressure at the center of the base. Similar base pressure profiles were observed by Reid and Hastings[8] for a cylindrical afterbody in a Mach 2.0 flow with a maximum rise in pressure of approximately 3% across the base. An area-weighted average of the current data across the base was performed to determine an average base pressure coefficient of −0.102.

Flowfield Velocity Measurements

Approach Flow Measurements

The boundary layer approaching the base corner separation point was measured at three axial stations upstream of the base. Figure 4 is a plot of the boundary layer profile obtained 1 mm upstream of the base corner along with a curve fit by Sun and Childs[20] for compressible, turbulent boundary layers. The boundary-layer properties derived from the curve fit are also shown in Fig. 4. The values for the dimensionless properties (H, Π, and C_f) are typical of those found in equilibrium, compressible, turbulent boundary layers.[21] To determine the integral properties, the mean density profile through the boundary layer was determined using the ideal gas equation of state and the assumptions of negligible radial pressure gradient, adiabatic wall, and a recovery factor of 0.89 as suggested by Kays and Crawford.[22] The freestream Mach number across the nozzle exit was measured by LDV to be 2.46 ± 1% (the corresponding approach velocity was U_1 = 567 m/s). Also, measured freestream turbulence intensities in the approach flow were less than 1%.

Centerline Measurements

The LDV measurements along the model centerline were taken in 5-mm increments from the base to the end of the viewing window in the test section. A plot of the mean axial velocity along the

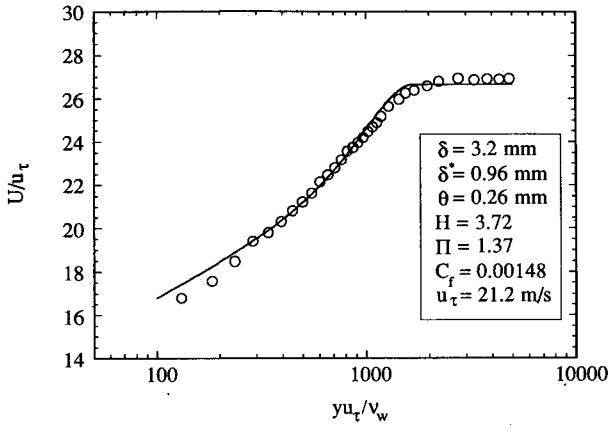

Fig. 4 Sun and Childs[20] curve fit of afterbody boundary-layer upstream of base corner.

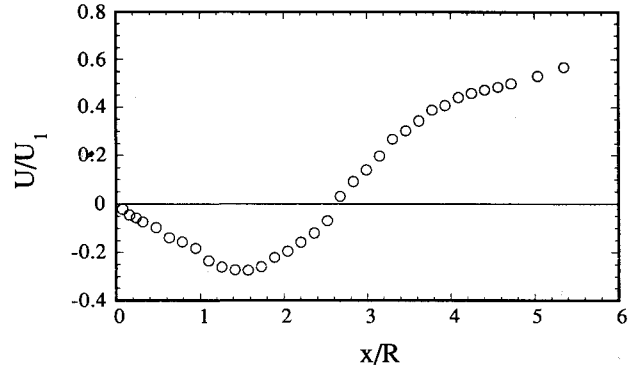

Fig. 5 Mean axial velocity along model centerline.

model centerline is shown in Fig. 5. The origin of the cylindrical coordinate system has been arbitrarily set at the center of the base with all axial distances positive downstream. The axial location where the data cross the $U = 0$ line clearly defines the rear stagnation point S since the other two measured velocity components are negligible along the centerline; this occurs at $x/R = 2.65$. The maximum reverse velocity occurs at $x/R \approx 1.5$ and takes a value of approximately 27% of the approach freestream velocity. In a similar experiment using LDV in subsonic flow (Mach 0.85) behind a circular cylinder, Delery[14] found the rear stagnation point located at 3.06 base radii downstream and a maximum reverse velocity of approximately 30% of the local freestream value located at $x/R = 1.8$. It is interesting to note that for both the supersonic and subsonic cases, the maximum reverse velocity occurs at a location approximately 57% of the distance from the base to the reattachment point. Merz et al.[23] found that for all Mach numbers from 0.1 to 0.9, the maximum reverse velocity was 35–40% of the freestream velocity and occurred at a distance 60% of the length to reattachment. The degree of wake redevelopment in the present experiments is indicated in Fig. 5 by the maximum positive centerline velocity which takes the value of 57% of the approach velocity ($M \approx 1.05$) at the farthest downstream station.

Near-Wake Mean Velocity Measurements

The mean velocity vector field in the near wake is shown in Fig. 6. In this and subsequent figures, the vertical axis has been expanded by 42% compared to the horizontal axis to more clearly show the features of the flowfield (the axial-to-radial aspect ratio of the actual LDV measurement grid is 4.27:1). To place the experimental data on a uniform grid for the vectors shown in Fig. 6, a simple linear interpolation in both x and r between the unequally spaced data was completed. The velocity vectors show clearly the dominance of the axial velocity on the overall mean velocity field. The turning of the mean flow through the base corner expansion fan, the relatively low-speed recirculation region, and the realignment of the mean flow with the axis downstream of reattachment (S) are clearly shown.

A contour plot of the Mach number distribution throughout the near wake is shown in Fig. 7. The steep velocity gradients through the initial portion of the shear layer are clearly evident in the figure. The spreading of the contour lines farther downstream is indicative of the growth of the shear layer prior to reattachment and, also, the wake development downstream. Note that the flow along the axis reaccelerates to sonic velocity at approximately five base radii downstream which is similar to the measurements of Neale et al.[13] in a Mach 3 base flowfield where the sonic point was located at $x/R = 5.1$. The maximum Mach number of the reverse flow is 0.48 and is located on the centerline at approximately $x/R = 1.5$. The gradual recompression of the outer flow is indicated by the decreasing Mach number contours in the upper right of the figure.

The mean radial velocity contours are shown in Fig. 8. The small values relative to the mean axial approach velocity once again show the dominance of the axial velocity in the near-wake flowfield. The closely spaced contours emanating from the base corner mark the turning of the mean flow through the expansion fan. As the outer inviscid flow approaches the axis of symmetry, the radial velocity continues to increase in magnitude, due to the axisymmetric effect, to a peak value of 22% of the mean approach velocity at a location approximately two base radii downstream. The location of flowfield realignment with the axis of symmetry appears to depend on whether the flow is supersonic or subsonic. The realignment process in the outer flow is shown in the upper right of Fig. 8 by the contour lines of decreasing magnitude and the relatively uniform flow region downstream of the last contour. However, closer to the axis of symmetry, a much slower realignment of the subsonic inner flow occurs, such that the mean radial velocity is appreciable out to $x/R = 4.5$. The mean tangential (swirl) velocity was also directly measured with the LDV system, and as expected, the magnitudes were negligible compared to the other two components.

Near-Wake Turbulence Measurements

The root-mean-square fluctuation velocities were directly measured in all three coordinate directions and will be presented in the form of turbulence intensities, σ/U_1. Figure 9 shows the axial tur-

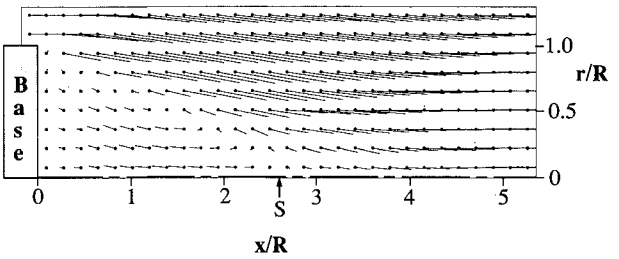

Fig. 6 Mean velocity vector field throughout near wake.

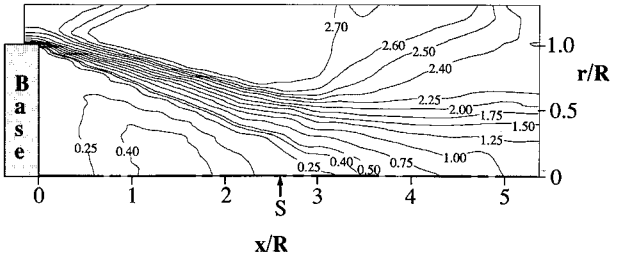

Fig. 7 Mach number contours.

bulence intensity contours throughout the near wake. The large increase in turbulent fluctuations from the outer freestream to the values in the shear layer and wake are apparent. A peak axial rms velocity fluctuation of 22% of the mean approach velocity occurs at a location 83% of the axial distance from the base to reattachment. Upstream of reattachment at any axial station, the radial location of the maximum axial turbulence intensity lies in the subsonic region of the shear layer. In contrast, Amatucci et al.[15] found peak levels of turbulence intensity near the sonic line in a two-dimensional, two-stream base flow. Throughout the recirculation region in the current study, the axial turbulence intensity is relatively constant except very close to the base where it is attenuated. Farther downstream as the shear layer transforms into a wake, the overall level of turbulent fluctuations diminishes, and a well-defined peak in the axial turbulence intensity profiles is no longer discernible.

Contours of constant radial turbulence intensity are shown in Fig. 10. The general trends follow closely those of the axial turbulence intensity, but the overall fluctuation levels are smaller. The peak radial velocity fluctuation is 15.6% of U_1 and occurs at roughly the same location as the peak axial fluctuation. The recirculation region contains a greater variation in radial turbulence intensity than axial turbulence intensity with a steady increase from the base to the reattachment point (not including the base effects at $x/R < 0.5$). The turbulence relaxation beyond reattachment is fairly slow with a uniform radial turbulence intensity across the inner portion of the wake as it develops.

The tangential turbulence intensity represents fluctuations from the mean swirl velocity which, as mentioned previously, is negligible for axisymmetric flows. Figure 11 is a plot showing the tangential turbulence intensity throughout the near wake. The overall level of fluctuations in the tangential direction is reduced compared to the axial turbulence intensity and is generally smaller than the radial fluctuations. The peak value of the tangential velocity fluctuations is 13.5% of U_1 and occurs near the shear layer reattachment point at $x/R = 2.65$. The greatest variation in tangential turbulence intensity occurs at the outer edges of the shear layer and wake, and the radial profiles do not exhibit the sharp peaks evident in the axial and radial turbulence intensities.

The ratio of the turbulence intensity contributions from each component gives a relative indication of the anisotropy in the normal stress field. In the current flow, the axial turbulence intensity dominates with peak values approximately 30–50% higher than

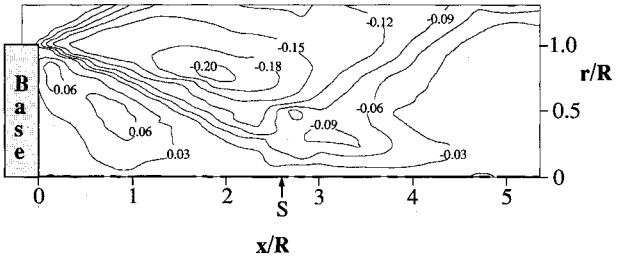

Fig. 8 Mean radial velocity contours, V_r/U_1.

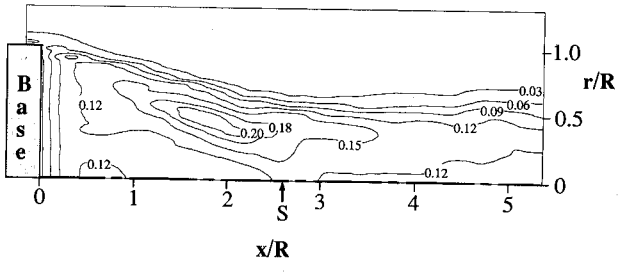

Fig. 9 Axial turbulence intensity contours, σ_u/U_1.

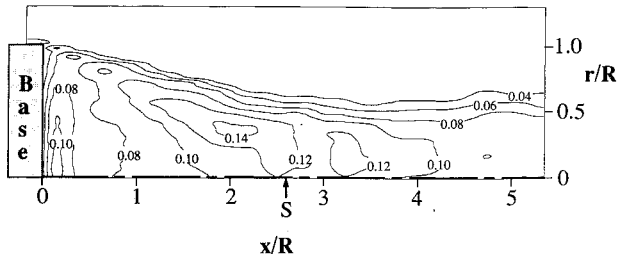

Fig. 10 Radial turbulence intensity contours, σ_{v_r}/U_1.

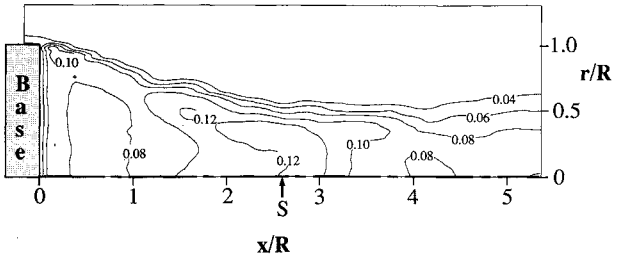

Fig. 11 Tangential turbulence intensity contours, σ_{v_t}/U_1.

the peak radial fluctuations and 60–70% higher than the peak tangential fluctuations in the shear layer where anisotropy is largest. The relative ordering of the peak turbulence intensity magnitudes (axial-radial-tangential) found in the current base flow experiments can be contrasted with the recent data from Gruber et al.[24] for a two-dimensional, compressible, constant-pressure mixing layer. In their study, the magnitude of the spanwise component of turbulence intensity exceeded the contribution from the transverse component by approximately 20% in the peak intensity region of the shear layer, probably due to the three-dimensional nature of the large-scale structures in the planar, compressible mixing layer. In axisymmetric flow, the tendency of the structures to grow asymmetrically (in the tangential direction) is most likely dampened by the more stringent axisymmetric conditions imposed by the mean flowfield. In incompressible, constant-pressure mixing layers, the spanwise component of turbulence intensity has been shown to be approximately equal to the transverse turbulence intensity.[25]

An important turbulence quantity often used to describe the overall level of turbulent fluctuations is the turbulent kinetic energy defined as

$$k = \tfrac{1}{2}\left(\sigma_u^2 + \sigma_{v_r}^2 + \sigma_{v_t}^2\right) \tag{2}$$

In these experiments, all three mean square fluctuations (normal stresses) have been directly measured. Figure 12 is a plot of the turbulent kinetic energy as measured throughout the near wake. Since the axial turbulence fluctuation levels dominate the flowfield, the contours of turbulent kinetic energy appear relatively similar to those of the axial turbulence intensity (Fig. 9). The turbulent kinetic energy grows rapidly after separation as the shear layer grows. Prior to reattachment, however, a maximum is reached and a subsequent decay to the relatively constant values in the wake occurs. Again, the sharp peaks in turbulent kinetic energy radial profiles occurring in the shear layer are nonexistent in the wake farther downstream. In the recirculation region, the level of turbulent kinetic energy is reduced by the lack of turbulence production due to small mean velocity gradients. The maximum turbulent kinetic energy measured in the near wake was 4.4% of U_1^2 and occurred at $x/R = 2.2$, or somewhat upstream of reattachment.

In the current experiments, both the axial-radial ($<u'v_r'>$) and axial-tangential ($<u'v_t'>$) Reynolds shear stresses have been measured directly. As expected, the axial-radial shear stress dominates the axial-tangential stress which is negligible throughout the near

wake. Figure 13 is a plot showing the axial-radial shear stress distribution downstream of the base. The shear stress peaks in the shear layer upstream of reattachment in approximately the same location as the peak in turbulent kinetic energy. Abu-Hijleh and Samimy[26] used LDV to investigate a supersonic shear layer reattaching onto a wall and found peak values of turbulent kinetic energy and Reynolds stress *downstream* of the reattachment location. The difference in the locations for the peak turbulence quantities between these experiments may possibly be attributed to the differences between solid wall and compliant surface reattachment.

The production of turbulent kinetic energy, defined as

$$P_k = -\langle u_i' u_j' \rangle \frac{\partial U_i}{\partial x_j} \tag{3}$$

provides a measure of the amount of kinetic energy transferred from the mean flow to the turbulence field. Investigating the distribution of P_k throughout the near wake provides insight into the structure of the turbulence field as well as establishing the role of turbulence production in different regions of the flow. In axisymmetric flow, only four of the nine production terms are nonzero which leaves the following expression for P_k:

$$P_k = -\sigma_u^2 \frac{\partial U}{\partial x} - \langle u' v_r' \rangle \left(\frac{\partial U}{\partial r} + \frac{\partial V_r}{\partial x} \right) - \sigma_{v_r}^2 \frac{\partial V_r}{\partial r} \tag{4}$$

which is plotted in Fig. 14 (to avoid clutter, only a reference contour label is shown; all other contours are equally spaced with values increasing by 0.02). Strong turbulence production is seen to occur immediately downstream of the separation point on the inner edge of the shear layer. This is not surprising as the mean velocity gradients are very large in this region. As the shear layer develops, the mean velocity gradients decrease but the Reynolds stresses increase (Figs. 9–13) such that the total production remains significant up to the reattachment point. Downstream of reattachment, however, the Reynolds stresses and mean velocity gradients both decrease rapidly resulting in a diminished level of turbulence production.

Since the total production of turbulent kinetic energy is merely the sum of the production terms for each Reynolds normal stress,

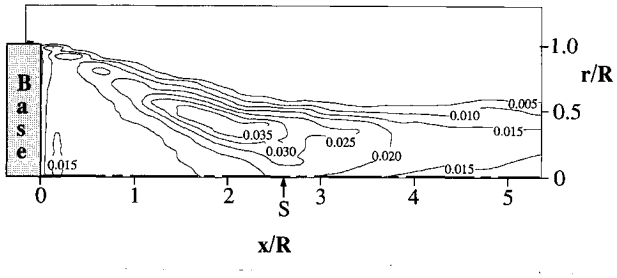

Fig. 12 Turbulent kinetic energy contours, k/U_1^2.

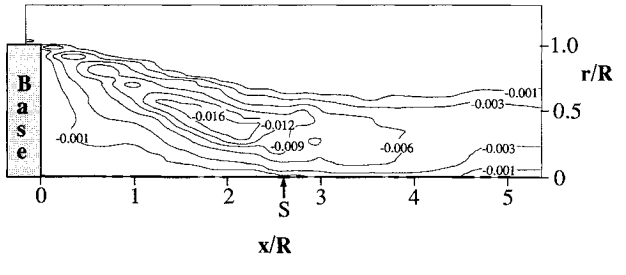

Fig. 13 Reynolds shear stress contours, $\langle u' v_r' \rangle / U_1^2$.

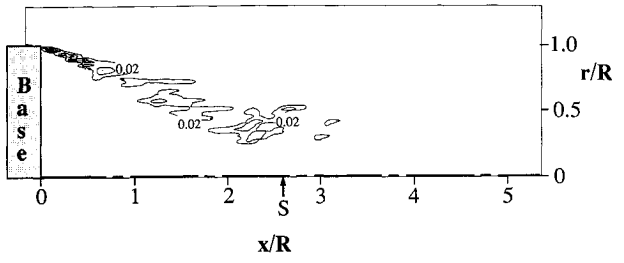

Fig. 14 Turbulence production contours, $P_k \cdot R/U_1^3$.

separating the total production expression into its individual components yields

$$P_k = P_u + P_{v_r} + P_{v_t} \tag{5}$$

where the individual production terms for each Reynolds normal stress are

$$P_u = -\sigma_u^2 \frac{\partial U}{\partial x} - \langle u' v_r' \rangle \frac{\partial U}{\partial r} \tag{6}$$

$$P_{v_r} = -\sigma_{v_r}^2 \frac{\partial V_r}{\partial r} - \langle u' v_r' \rangle \frac{\partial V_r}{\partial x} \tag{7}$$

$$P_{v_t} = 0 \tag{8}$$

From the current experiments, the relative magnitudes of each term indicate that $P_u \gg P_{v_r} > P_{v_t}$. Consequently, the majority of the energy exchange between the mean flow and the turbulence field occurs through the axial component of the Reynolds normal stress. On the other hand, the radial and tangential components must receive their kinetic energy from other sources such as pressure-velocity interactions or momentum transport by turbulent velocity fluctuations. Therefore, the relative ordering of the Reynolds normal stresses ($\sigma_u^2 > \sigma_{v_r}^2 > \sigma_{v_t}^2$) is consistent with the amount of turbulence production that each component receives from the mean flow.

Summary and Conclusions

The turbulent near wake of a circular cylinder aligned with a supersonic flow has been investigated using nonintrusive measurement techniques. The main objective of these experiments is to increase the understanding of the complex fluid dynamic phenomena that occur in supersonic base flowfields by the use of detailed quantitative data gathered throughout the near wake. Specifically, afterbody and base pressure distributions, mean velocities, turbulence intensities, and Reynolds shear stresses have been obtained; these data have been tabularized on a floppy disk which is available from the authors. As a result of data analysis, the following conclusions concerning the near-wake flowfield can be made:

1) The mean static pressure profile across the base is relatively uniform with an average base pressure coefficient of −0.102.

2) The maximum reverse velocity along the wake centerline reached 27% of the mean approach velocity, or Mach 0.48, and occurs approximately 57% of the distance from the base to the reattachment point (located at x/R = 2.65). Along the centerline, the axial and radial turbulence intensities peak near the reattachment point and decay as the wake develops downstream.

3) The recirculating flow is generally characterized by small mean velocity gradients and relatively uniform turbulence intensities.

4) The separated shear layer is found to contain steep radial velocity gradients and sharp peaks in turbulence intensity in the subsonic region. Beyond reattachment, the sharp peaks decay toward nearly uniform turbulence intensities across the redeveloping wake.

5) Peak values of turbulent kinetic energy and axial-radial shear stress are located in the subsonic region of the shear layer upstream of reattachment. This is in contrast to earlier results on compressible shear layer reattachment onto a solid surface which indicate peak levels at or downstream of the reattachment point. The production of turbulent kinetic energy peaks immediately downstream of separation along the inner edge of the shear layer.

Acknowledgment

This work was supported by the U.S. Army Research Office (Contract DAAL03-90-G-0021) with Thomas L. Doligalski serving as Contract Monitor.

References

[1]Rollstin, L., "Measurement of Inflight Base Pressure on an Artillery-Fired Projectile," AIAA Paper 87-2427, Aug. 1987.

[2]Delery, J., and Wagner, B., "Results of GARTEUR Action Group AG09 on Flow Past Missile Afterbodies," *Proceedings of the AGARD/FDP Symposium on Missile Aerodynamics*, Friedrichshafen, Germany, April, 1990.

[3]Peace, A. J., "Turbulent Flow Predictions for Afterbody/Nozzle Geometries Including Base Effects," *Journal of Propulsion and Power*, Vol. 7, No. 3, 1991, pp. 396–403.

[4]Sahu, J., "Supersonic Flow Over Cylindrical Afterbodies with Base Bleed," AIAA Paper 86-0487, Jan. 1986.

[5]Wilmoth, R. G., and Putnam, L. E., "Subsonic/Transonic Prediction Capabilities for Nozzle/Afterbody Configurations," AIAA Paper 84-0192, Jan. 1984.

[6]Korst, H. H., "A Theory for Base Pressures in Transonic and Supersonic Flow," *Journal of Applied Mechanics*, Vol. 23, No. 4, 1956, pp. 593–600.

[7]Zumwalt, G. W., "Analytical and Experimental Study of Axially-Symmetric Supersonic Base Pressure Problem," Ph.D. Thesis, Dept. of Mechanical Engineering, Univ. of Illinois at Urbana-Champaign, Urbana, IL, 1959.

[8]Reid, J., and Hastings, R. C., "Experiments on the Axi-Symmetric Flow Over Afterbodies and Bases at M = 2.0," Royal Aircraft Establishment, RAE Rept. Aero. 2628, Farnborough, England, UK, 1959.

[9]Badrinarayanan, M. A., "An Experimental Investigation of Base Flows at Supersonic Speeds," *Journal of the Royal Aeronautical Society*, Vol. 65, July 1961, pp. 475–482.

[10]Demetriades, A., "Mean-Flow Measurements in an Axisymmetric Compressible Wake," *AIAA Journal*, Vol. 6, No. 3, 1968, pp. 432–439.

[11]Hawkins, R., and Trevett, E., "Changes in the Flow at the Base of a Bluff Body Due to a Disturbance in its Wake," AGARD Rept. 539, May 1966.

[12]Gaviglio, J., Dussauge, J. P., Debieve, J. F., and Favre, A., "Behavior of a Turbulent Flow Strongly Out of Equilibrium at Supersonic Speeds," *Physics of Fluids*, Vol. 20, No. 10, 1977, pp. 179–192.

[13]Neale, D. H., Hubbartt, J. E., Strahle, W. C., and Wilson, W. W., "Effects of External Compression on an Axisymmetric Turbulent Near Wake," *AIAA Journal*, Vol. 16, No. 9, 1978, pp. 940–947.

[14]Delery, J., "ONERA Research on Afterbody Viscid/Inviscid Interaction with Special Emphasis on Base Flows," *Proceedings of the Symposium on Rocket/Plume Fluid Dynamic Interactions, Vol. III—Flow Fields*, Univ. of Texas at Austin, Austin, TX, 1983; also Fluid Dynamics Labs. Rept. 83–104, April 1983.

[15]Amatucci, V. A., Dutton, J. C., Kuntz, D. W., and Addy, A. L., "Two-Stream, Supersonic, Wake Flowfield Behind a Thick Base, Part I: General Features," *AIAA Journal*, Vol. 30, No. 8, 1992, pp. 2039–2046.

[16]Heltsley, F. L., Walker, B. J., and Nichols, R. H., "Transonic Nozzle-Afterbody Flow Field Measurements Using a Laser Doppler Velocimeter," AGARD CP-348, Sept. 1983.

[17]Bloomberg, J. E., "An Investigation of Particle Dynamics Effects Related to LDV Measurements in Compressible Flows," M.S. Thesis, Dept. of Mechanical and Industrial Engineering, Univ. of Illinois at Urbana-Champaign, Urbana, IL, 1989.

[18]Samimy, M., and Lele, S. K., "Motion of Particles with Inertia in a Compressible Free Shear Layer," *Physics of Fluids A*, Vol. 3, No. 8, 1991, pp. 1915–1923.

[19]Herrin, J. L., and Dutton, J. C., "An Investigation of LDV Velocity Bias Correction Techniques for High-Speed Separated Flows," *Experiments in Fluids*, Vol. 15, No. 4–5, pp. 353–363.

[20]Sun, C. C., and Childs, M. E., "A Modified Wall Wake Velocity Profile for Turbulent Compressible Boundary Layers," *Journal of Aircraft*, Vol. 10, No. 6, 1973, pp. 381–383.

[21]Fernholz, H. H., and Finley, P. J., "A Critical Commentary on Mean Flow Data for Two-Dimensional Compressible Turbulent Boundary Layers," AGARDograph No. 253, May 1980.

[22]Kays, W. M., and Crawford, M. E., "The Turbulent Boundary Layer for a Gas with Variable Properties," *Convective Heat and Mass Transfer*, 2nd ed., McGraw-Hill, New York, 1980, pp. 305–309.

[23]Merz, R. A., Page, R. H., and Przirembel, C. E. G., "Subsonic Axisymmetric Near-Wake Studies," *AIAA Journal*, Vol. 16, No. 7, 1978, pp. 656–662.

[24]Gruber, M. R., Messersmith, N. L., and Dutton, J. C., "Three-Dimensional Velocity Field in a Compressible Mixing Layer," *AIAA Journal*, Vol. 31, No. 11, pp. 2061–2067.

[25]Bell, J. H., and Mehta, R. D., "Interaction of a Streamwise Vortex with a Turbulent Mixing Layer," *Physics of Fluids A*, Vol. 2, No. 11, 1990, pp. 2011–2023.

[26]Abu-Hijleh, B., and Samimy, M., "An Experimental Study of a Reattaching Supersonic Shear Layer," AIAA Paper 89-1801, June 1989.